Harmful Algae 99 (2020) 101927

Contents lists available at ScienceDirect

Harmful Algae

journal homepage: www.elsevier.com/locate/hal

Dynamics of an intense *Alexandrium catenella* red tide in the Gulf of Maine: satellite observations and numerical modeling

Yizhen Li, Ph.D. [a,*], Richard P. Stumpf [b], D.J. McGillicuddy Jr. [c], Ruoying He [d]

[a] CSS Inc. under contract to NOAA National Centers for Coastal Ocean Science, 1315 East West Highway, Silver Spring, MD 20910
[b] NOAA National Centers for Coastal Ocean Science, 1315 East West Highway, Silver Spring, MD 20910
[c] Department of Applied Ocean Physics and Engineering, Woods Hole Oceanographic Institution, Woods Hole, 02543
[d] Department of Marine, Earth, and Atmospheric Sciences, North Carolina State University, Raleigh, NC, 27695

ARTICLE INFO

Keywords:
Red water
Bloom patches
Cell accumulation
Coastal upwelling
Upward swimming

ABSTRACT

In July 2009, an unusually intense bloom of the toxic dinoflagellate *Alexandrium catenella* occurred in the Gulf of Maine. The bloom reached high concentrations (from hundreds of thousands to one million cells L^{-1}) that discolored the water and exceeded normal bloom concentrations by a factor of 1000. Using Medium Resolution Imaging Spectrometer (MERIS) imagery processed to target chlorophyll concentrations (>2 μg L^{-1}), patches of intense *A. catenella* concentration were identified that were consistent with the highly localized cell concentrations observed from ship surveys. The bloom patches were generally aligned with the edge of coastal waters with high-absorption. Dense bloom patches moved onshore in response to a downwelling event, persisted for approximately one week, then dispersed rapidly over a few days and did not reappear. Coupled physical-biological model simulations showed that wind forcing was an important factor in transporting cells onshore. Upward swimming behavior facilitated the horizontal cell aggregation, increasing the simulated maximum depth-integrated cell concentration by up to a factor of 40. Vertical convergence of cells, due to active swimming of *A. catenella* from the subsurface to the top layer, could explain the additional 25-fold intensification (25 × 40=1000-fold) needed to reach the bloom concentrations that discolored the water. A model simulation that considered upward swimming overestimated cell concentrations downstream of the intense aggregation. This discrepancy between model and observed concentrations suggested a loss of cells from the water column at a time that corresponded to the start of encystment. These results indicated that the joint effect of upward swimming, horizontal convergence, and wind-driven flow contributed to the red water event, which might have promoted the sexual reproduction event that preceded the encystment process.

1. Introduction

The toxic dinoflagellate *Alexandrium catenella* (previously *Alexandrium fundyense*, Prud'homme van Reine, 2017) has a major economic impact on molluscan shellfisheries on the coastal northwest Atlantic due to the risk of paralytic shellfish poisoning (PSP, Anderson et al., 1990), especially in the Gulf of Maine (GOM, Fig. 1). As an example, in 2005, in the state of Massachusetts alone, economic losses of as much as $50 million were caused by an extensive *A. catenella* bloom (Jin and Hoagland, 2008). The *Alexandrium* blooms in the Gulf of Maine start in spring, typically April, and persist into summer when the remainder of the cells may encyst. These cysts settle into the sediment to over-winter (Anderson, 1998).

While these blooms are described as "red tide", this is typically a misnomer. PSP, which results from shellfish that have accumulated saxitoxins, can occur with low cell concentrations of only several hundred cells L^{-1}. During bloom conditions (Smayda, 1997), *A. catenella* rarely reaches concentrations of more than a few thousands cells L^{-1} (equivalent to much less than 1 μg L^{-1} chlorophyll-*a*), and is thus insufficient to discolor the water. In contrast, *Karenia brevis*, the dinoflagellate that causes Gulf of Mexico "red tide", has a similar size but a toxin risk starting at 5000 cells L^{-1}, and typically accumulates to $>10^5$ cells L^{-1} (equivalent to 1 μg L^{-1} chl-a) at which concentration *K. brevis* does discolor the water.

Understanding the *A. catenella* bloom in the Gulf of Maine, especially at seasonal to interannual time scales has been a major focus during the

* Corresponding author.
E-mail addresses: Yizhen.Li@noaa.gov, Yizhen.Li@noaa.gov (Y. Li).

https://doi.org/10.1016/j.hal.2020.101927
Received 3 April 2020; Received in revised form 15 September 2020; Accepted 16 October 2020
Available online 26 October 2020

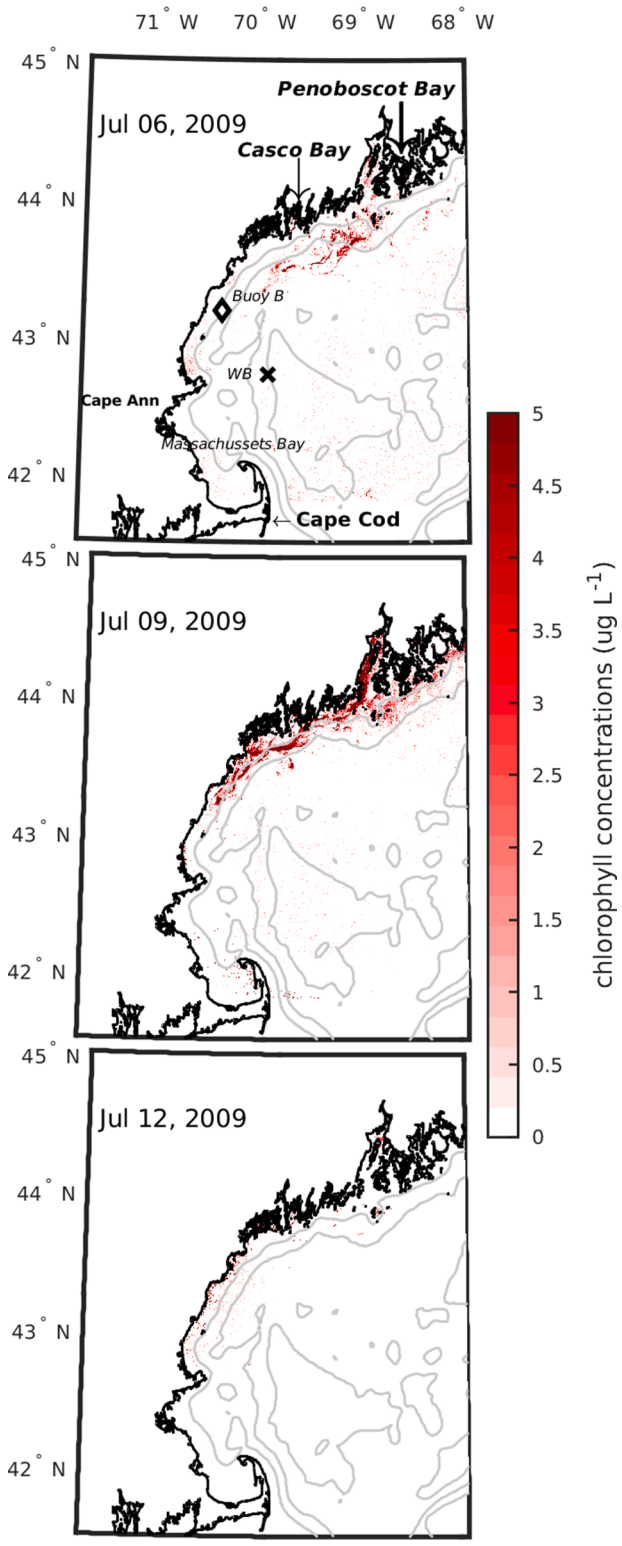

Fig. 1. MERIS-derived relative chlorophyll concentrations (ug L^{-1}) for July 6, 9, and 12 of 2009 during the red water event. Gray contours highlight 50, 100, and 200-m isobaths. Important geographic locations are labeled on the top panel. Black diamond represents the location of NERACOOS buoy B where wind measurements were collected (shown in Fig.2), and black cross stands for the Wilkinson Basin (WB) location of the sediment trap where time series of cyst data was collected, as described in Pilskaln et al., 2014 and McGillicuddy et al., 2014. (For interpretation of the references to colour in this figure legend, the reader is referred to the web version of this article.)

past two decades. Kleindinst et al. (2014) classified the bloom into three categories ('limited','moderate' and 'extensive') by the extent of the annual shellfish bed closure for coastal New England states due to PSP. The most extensive recent bloom occurred in spring and summer 2005, causing extensive shellfish bed closure along the coast (Anderson et al., 2005a). A large deposition of cysts in the fall prior to the bloom year may be crucial for the bloom initiation (Anderson et al., 2005b). Combining in situ observations with coupled physical-biological numerical modeling efforts, McGillicuddy et al. (2005) provided insights into the mechanisms responsible for bloom initiation and development. In that study, seasonal evolution of the bloom was found to be temperature-dependent during bloom initiation and more nutrient-dependent in June-August. Environmental pressures, like nutrient depletion, may also influence the timing and magnitude of cell removal by encystment (McGillicuddy et al., 2005).

The results of physical-biological models have suggested that cyst abundance in the western Gulf of Maine may serve as the first-order predictor of next year's bloom (He et al., 2008; Li et al., 2009). Other environmental factors modify the scale of the bloom. The major bloom in 2005 was associated with strong downwelling in May, and warmer-than-usual temperature in the western Gulf of Maine (He and McGillicuddy, 2008). In contrast, a moderate bloom took place in 2006 and was associated with normal wind and hydrodynamic conditions (Li et al., 2009). In 2010, a weaker-than-expected bloom occurred, despite high cyst abundance the previous fall. The suppression of the bloom was largely due to nutrient-depletion as a result of the intrusion of an anomalous water mass into the Gulf of Maine as well as an earlier-than-normal spring bloom of the phytoplankton population. The combined physical, biological, and chemical properties work in concert to influence the bloom after excystment occurred (McGillicuddy et al., 2005, 2011; Li et al., 2014).

Downwelling in the Gulf of Maine has previously been presented as a factor in dinoflagellate bloom development, as downwelling can sweep cells into the coastal plume, which leads to increased concentration near the coast (Franks and Anderson, 1992; McGillicuddy et al., 2003). A similar effect of downwelling circulation 'sweeping' cells to the coast was described for *K. brevis* blooms along the Texas coast (*Hetland* et al., 2007). In 2009, downwelling-favorable winds occurred from mid-June to early July, a duration not seen during the same summer periods of other recent years. A drifter released near Portsmouth followed a track consistent with this downwelling tendency. The red water event in early July followed the persistent downwelling-favorable winds (Fig. 2, highlighted period is embraced by arrows), which is unusual during mid-summer.

A unique behavior of dinoflagellates is the ability to swim actively towards light and/or nutrients (Kamykowski et al., 1992). Swimming behavior leading to changes in vertical concentration can be observed from Lagrangian optical drifters (Schofield et al., 2006), and from satellite observations (Tyler and Stumpf, 1989; Choi et al., 2013; Lou and Hu, 2014). Swimming behavior coupled with wind-induced transport, can accumulate cells at frontal boundaries (Le Fèvre, 1987). The combination of physical accumulation and vertical swimming by dinoflagellates has been well demonstrated to facilitate cell aggregation (Tyler and Seliger, 1981; Franks, 1992; Litaker et al., 2002; Janowitz and Kamykowski, 2006; Stumpf et al., 2003, 2008). For example, chlorophyll *b*iomass of *K. brevis* along Southwest Florida can increase 10-fold in a day along a front (Stumpf et al., 2008). Along the Texas coast, while wind-driven flow transports *K. brevis* cells to the coast, upward swimming keeps the cells near the surface so they do not exit through bottom return flow, thereby leading to cell accumulation nearshore (Hetland et al., 2007).

A. catenella is an energetic swimmer with a swimming to sinking velocity ratio of >10:1, and is known to be highly adapted for frontal zones compared to other types of dinoflagellates (Carreto et al., 1986; Smayda, 2002). Offshore frontal systems can serve as sources for seeding dinoflagellate blooms, i.e., the 'pelagic seed bank' (Smayda, 2002). Cells

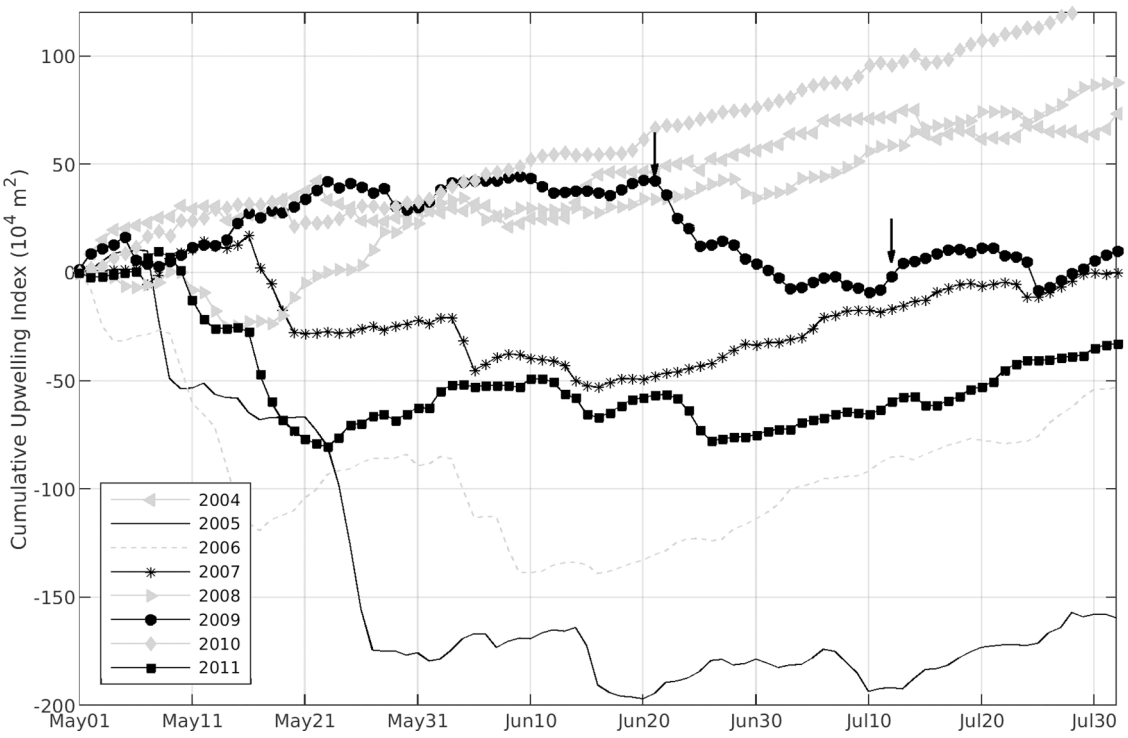

Fig. 2. Time series of cumulative upwelling indices (CUI) for 2004–2011 at NERACOOS buoy B in the western Gulf of Maine, initialized from May 01 of each year. The unit for the indices is 10^4 m^2. Vertical arrows bracket the period of strong downwelling during the late June to mid July of 2009.

entrained into coastal currents can also seed offshore habitats (Franks and Anderson, 1992). A physical front is defined as a narrow zone of enhanced horizontal gradient of physical properties, usually a density front produced by salinity in coastal zones (Yentsch and Phinney, 1996). Temperature may differ across these salinity fronts, so in certain cases satellite sea surface temperature (SST) may indicate coastal fronts. One study did find that thermal fronts and PSP toxins were spatially related in the coastal region of the Gulf of Maine (Luersson et al., 2005), although such thermal fronts are typically undetectable in spring and summer (Ullman and Cornillon, 1999). Physical/density fronts in the Gulf of Maine are associated with salinity changes (Incze and Yentsch, 1981; Stumpf and Goldschmidt, 1992; Hetland et al., 2015). Compared to physical fronts, biological fronts are more complex, often associated with biological enhancement, and small- and meso- scale blooms featuring spatial patterns that were not generally observable in SST fields (Belkin and O'Reilly, 2009).

Although the interannual variability of the bloom has been described with in situ measurements, the use of satellite imagery for *A. catenella* research has been rather limited. There are some practical reasons for the lack of remote sensing applications. *A. catenella* is only a small component of the phytoplankton assemblage in the Gulf of Maine, thus normally not the major contributor to the biomass (Love et al., 2005). If patches of high biomass blooms occurred in the past, we have lacked high-resolution satellite products and concurrent field observations to identify these patches. July 2009 was the first time we had satellite images concurrent with field observations to confirm a *A. catenella* bloom event that affected water color. During this time period, *A. catenella* in the Gulf of Maine developed a strong bloom that reached concentrations that visibly discolored the water. McGillicuddy et al. (2014) used Medium Resolution Imaging Spectrometer (MERIS) 1-km data to show broad spatial and temporal patterns of chlorophyll in the Gulf of Maine that could be associated with *A. catenella*. However, identification of the bloom patches is not possible with this low-resolution satellite data.

The 2009 Gulf of Maine bloom diminished shortly after the shipboard observations of discolored water (McGillicuddy et al., 2014). Details of the initiation and disappearance of the extreme bloom were not possible with the limited in situ data. In this paper, we seek to understand the coupling of wind-induced downwelling (convergence) and upward swimming in aggregating cells during the red water event. To do this, we synthesize additional observational and satellite data, along with numerical model simulations that incorporate finer-scale spatial-temporal behavior of these blooms to better understand the process.

2. Methods

Satellite data processing. Satellite data sets have been used to aid in understanding the dynamics of other dinoflagellate blooms that develop to high concentrations (e.g., Tyler and Stumpf, 1988; Raine et al., 2001; Stumpf et al., 2008). Of the several ocean color sensors that were available during the study period, MERIS, on the European Space Agency's Envisat-1, provided the highest resolution with bands suitable for discriminating chlorophyll in coastal optically complex waters. Level-1 MERIS full-resolution imagery (nominal 300 m resolution) was obtained from the NASA Ocean Color web site (oceancolor.gsfc.nasa.gov) and processed with the NASA's SeaDAS software version 7.0.1 (NASA, 2013) to obtain Rayleigh-corrected albedo (standard "*rho_s*" or ρ_s product). Products were mapped to universal transverse Mercator (UTM) at 300 m with nearest neighbor interpolation. The ρ_s was used to allow subsequent analysis without the negative radiances that standard atmospheric corrections can produce in highly colored waters, which are particularly likely to occur in dense surface accumulations of cells.

The Gulf of Maine has both case I (bio-optically simple) and case II waters. Examining an intense bloom requires a robust algorithm that specifically targets chlorophyll (including high concentrations), while avoiding ambiguities due to colored dissolved organic matter, which is a significant issue with plumes originating from Maine's tannin-rich rivers (Balch et al., 2016; Yentsch and Phinney, 1997). Estimation of cell concentration was based on chlorophyll concentration estimated using a ratio of 709 nm (near-infrared) and 665 nm (red) bands (Gilerson et al., 2008; Moses et al., 2012). The 665 nm band is positioned on a strong absorption zone of chlorophyll-a; the near-infrared is insensitive to

absorption by all substances in water, except the water itself. Near-infrared/red ratios can quantify chlorophyll in photosynthetic dinoflagellate blooms, even with less sensitive near-infrared measurements at wavelengths above 720 nm (Stumpf and Tyler, 1988). This 709 nm algorithm detects chlorophyll concentration within 1-m of the surface, which is compatible with the positively phototactic (upward) swimming of *A. catenella* (Anderson and Stolzenbach, 1985).

For atmospheric correction, the 885 nm band was used presuming a maritime atmosphere (Stumpf and Pennock, 1989). Errors resulting from aerosol type in this type of algorithm are small and systematic only over broad scales (Stumpf and Tyler, 1988). Combining the chlorophyll algorithm and atmospheric correction gives chlorophyll (C):

$$C = a[(\rho_s(709) - \rho_s(885)) / (\rho_s(665) - \rho_s(885))] - -b \quad (1)$$

using the Gilerson coefficients of $a = 61\ \mu g\ L^{-1}$and $b = 38\ \mu g\ L^{-1}$. The algorithm is insensitive to chlorophyll-$a < 2\ \mu g\ L^{-1}$. Gilerson et al. (2008) and Stumpf and Tyler (1988) indicated the linear ratio algorithm with these spectral bands is valid to chlorophyll-a >100 μg L^{-1}. We compared our results with the MCI (Maximum Chlorophyll Index)-derived counterpart (Gower et al., 2005). The MCI (not shown) only detected the densest concentrations in some of the high concentration patches, likely because the MCI is only sensitive to chlorophyll concentrations greater than about 10 μg L^{-1} (Binding et al., 2013). The Gilerson method detected the spatial distribution of the bloom over a much larger area, giving much more information on the bloom distribution.

To further understand the process of the coherence variance of water mass boundaries (and associated density fronts) with biological patches, spectral marine absorption products using the Quasi-Analytical Algorithm at 443 nm (QAA, Lee et al., 2002, 2009) by both MERIS and Moderate Resolution Imaging Spectro-radimeter (MODIS) were processed to reflect the riverine sources. Satellite-derived absorption (a_{dg}) produced by colored dissolved organic and particulate matter, i.e., CDOM and detrital material) has been shown to capture salinity variations near the coast, which would represent coastal low salinity water masses (e.g., Stumpf and Goldschmidt, 1992; Balch et al., 2004; Bai et al., 2013; Salisbury et al., 2011). As supplemental analysis, to determine if the variations in biological patches were associated with thermal gradients, sea surface temperature (SST) imagery from the MODIS on NASA's Aqua and Terra satellites was processed and subsequently mapped at 1.1 km resolution for the same area and time of interest. No SST fronts were found to be associated with the biological patches in the coastal area. Perceptually uniform color scales (viridis on QAA and SST) were used on the satellite imagery to allow visualization of gradients or fronts (Liu and Heer, 2018).

Cumulative Upwelling Index. To describe surface wind conditions in June-July 2009, we computed the cumulative upwelling index (CUI) at NERACOOS buoy B. The surface wind forcing was quantified using an Upwelling Index ($UI = \tau_x/\rho f$, i.e., the offshore component of the surface Ekman transport), following the method of Schwing et al.(1996), where the along-shore component of wind stress $\tau_x$is calculated using the Large and Pond (1981) formulation, $\rho$is the water density,and $f$is the local Coriolis parameter. Positive (negative) UI represents upwelling (downwelling) favorable wind conditions, respectively. The cumulative UI (CUI) was then computed by integrating the resulting UI over time (i.e.,$CUI = \int_{t0}^{t1} UIdt$) between May 1 and August 1 of each year. The slope of CUI is particularly informative, in that the most upwelling favorable wind conditions are represented by the steepest rising trend in CUI. In contrast, a declining trend in CUI indicates that downwelling favorable winds (negative UI) become more dominant. Similar approaches have been applied to quantify wind-induced coastal transport events at various oceanic regions (e.g., Hyun and He, 2010; Li et al., 2014; McGillicuddy et al., 2014).

3. Coupled physical-biological model

We used a coupled physical-biological model described by Li et al. (2009) to hindcast time-space continuous hydrodynamics and *A. catenella* cell fields during the red tide events between June-July 2009.

The circulation module is based on the Regional Ocean Modeling System (ROMS, http://www.myroms.org/), a free-surface, hydrostatic, primitive-equation model. ROMS is formulated in vertically stretched, terrain-following coordinates (Shchepetkin and McWilliams, 2005). For the hydrodynamic open boundary conditions (OBCs), a multi-nested configuration was implemented to downscale global data assimilative Hybrid Coordinate Ocean Model (HYCOM, http://hycom.rsmas.miami.edu/dataserver) solutions to a shelf-wide ROMS model and subsequently to the GOM ROMS model (He et al., 2008) via a one-way nesting approach. The method of Marchesiello et al. (2001) was applied to prescribe boundary values of tracers and baroclinic velocity. For the free surface and depth-averaged velocity boundary conditions, the method of Flather (1976) was used with the external values provided by the "parent" model. Because HYCOM does not consider tides, we also superimposed along open boundaries tidal (M_2, S_2, N_2, K_2, K_1, O_1, Q_1) sea level and depth-averaged velocity using harmonics derived from an ADCIRC simulation of the western Atlantic (Luettich et al., al.,1992). The Mellor-Yamada (1982) closure scheme and the quadratic drag formulation were applied to compute the vertical turbulent mixing and the bottom friction specification. The GOM ROMS has a spatial resolution of 3 km (2 km) in the along-shore (cross-shelf) direction, and 36 terrain-following vertical levels that have higher resolutions near the surface and bottom to better resolve boundary layers.

The biological module is a single-component model (Anderson et al., 2005a; Stock et al., 2005; McGillicuddy et al., 2005; He et al., 2008; Li et al., 2009). The purpose of this paper is to better understand the impact of wind and upward swimming on the red water event during a short duration of time, and thus both growth (light and nutrient dependent) and mortality and cyst germination are neglected herein. The module can be expressed as a single advection-diffusion equation:

$$\frac{\partial C}{\partial t} + \nabla\cdot((\vec{u} + W_a)C) = \nabla\cdot K\nabla C \quad (2)$$

Local Rate of Change Advection Diffusion where C is the cell concentration of *A. catenella*; $\vec{u}$and $W_a$are the fluid velocity and *A. catenella*upswimming velocity, taken as 10 m day^{-1} (Kamykowski et al., 1992) throughout the model simulation in the ocean interior. K is the diffusivity coefficient from the physical circulation model. On the left hand side of the equation, $\frac{\partial C}{\partial t}$stands for the time rate of change for the cell concentration C, and $\nabla\cdot((\vec{u} + W_a)C)$stands for the advection flux of concentration due to both physical circulation and directional upward swimming. The right hand side stands for the diffusion of the cells.

A. catenella cell concentrations (in relative units) were initialized at surface layer based on MERIS satellite data (in the form of cell density) in July 06, 2009. A no-gradient boundary condition was applied to cell concentrations along the model open boundaries. The boundary setting assumes little impact on the internal solutions (cells are conserved in all models, see conservation calculation in Fig. S1) because the study domain is away from the boundaries and the simulation is for a short period.

For both shelf-scale ROMS and GOM ROMS hindcasts, surface atmospheric forcing, including cloud fraction, precipitation, surface pressure and humidity, air temperature, surface wind, and shortwave radiation were obtained from the National Center for Environmental Prediction (NCEP), North America Regional Reanalysis (NARR). Both NARR wind (not shown) and wind at NERACOOS (http://www.neracoos.org/) buoy B show persistent downwelling-favorable winds during June 20-early July. Sporadic reversals occurred during 3–6 July, then a downwelling-favorable wind event occurred from July 6–9,

followed by an upwelling during 9–12 July; these can be seen in the cumulative upwelling index (CUI, Fig. 2). Spatial and temporal resolutions of these forcing fields are 32 km and 3 h, respectively. They were applied in the standard bulk flux formulation to derive wind stress and net surface heat flux needed by the simulations. GOM ROMS also incorporates river runoff as an important forcing agent, for which observed daily river runoff time series from United States Geological Survey (USGS) were used to provide freshwater input to the model.

Given the nature of the one-way nesting, model hindcasts were performed in sequential order. The nested shelf-scale ROMS hindcast was performed first, in which only the hydrodynamics were computed; then with the initial condition and OBCs from shelf-scale ROMS, the nested GOM ROMS hindcast was carried out, in which both hydrodynamics and the *A. catenella* cell concentration were simulated simultaneously.

Details of the numerical simulations are summarized in Table 1. For the short simulation of interest, we set up three model runs to examine the relative contribution of upward swimming and surface wind forcing. (1) In the first run (Exp.1, Swimming+Wind), we assumed a steady upward swimming over the water column forced by realistic surface wind forcing; (2) In the second simulation (Exp.2, No Swimming+Wind), wind forcing remained the same, while upward swimming of the cells was switched off. The experiment thus became a passive tracer simulation; (3) In the third simulation (Exp.3, Swimming+No Wind), we assumed a steady swimming, with wind forcing turned off to contrast with Exp.1 that included a downwelling event during July 6–12. (4) For a follow up examination of model sensitivity, a model was initiated from June 25, 2009 with uniform concentration everywhere to investigate the impact of upward swimming on the cell accumulation.

4. Results

4.1. Satellite observations

Chlorophyll. In the central Gulf of Maine, satellite estimates of chlorophyll-a (chl-a) with this algorithm were < 2 μg L^{-1}, which is typical for the area (Fig. 1). The coastal zone had estimated chl-a concentration of 2–8 μg L^{-1}. In some areas, the estimated concentrations in these areas were > 8 μg L^{-1}, with narrow bloom patches having chl-a accumulations estimated at 50–100 μg L^{-1}.

McGillicuddy et al. (2014) reported cell concentrations of 324,000 to 2.5 million cells L^{-1} in a bloom patch offshore of Portsmouth on July 10. Based on the results of Anderson et al. (1990), *A. catenella* has a chl-a content that varies around 20 pg chl-a cell^{-1}. Accordingly, 1 million cells L^{-1} would have about 20 μg L^{-1}, 324,000 and 2.5 million cells would have about 6.5 μg L^{-1} and 50 μg L^{-1} of chl-a, respectively. The measured cell counts and satellite ocean-color estimates in the area are consistent within 50% of that range, which is about the variability inferred from Anderson et al. (1990). In contrast, samples taken on a transect off Cape Ann on July 12 peaked at <10,000 cells L^{-1}. While this concentration is high for *A. catenella*, it would correspond to chl-a of < 1 μg L^{-1}, barely resolvable against the background concentration in the coastal Gulf of Maine, and consistent with satellite estimates of < 2 to 3 μg L^{-1} in that area on the same day.

On July 6, dense bloom patches (Fig. 1) spanned from the mouth of Penobscot Bay southwestward. The downstream portion and the center of mass (CoM) of the bloom patches was offshore of 100-m isobath near Casco Bay (Fig. 3). Three days later, on July 9, the patches of elevated chl-a were more extensive and moved closer to the coast (within the 50-m isobath), while further extending southwestward to New Hampshire waters. The CoM in the July 9 MERIS image was also located closer to shore (than July 6) and inside the 50-m isobath near the northern end of the Casco Bay (Fig. 3). By July 12, the patches disappeared, chlorophyll concentrations greatly decreased, and low chlorophyll concentrations persisted in the coastal zone through the rest of the month.

QAA marine absorption due to CDOM. The coastal plume of the Gulf of Maine is a dominant feature in the coastal current system (e.g., Hetland and Signell, 2005; Pettigrew et al., 2005; Keafer et al., 2005). The plume contains a high-concentration of materials (e.g., CDOM) from the riverine sources that visible from satellite (Balch et al., 2016). The QAA product provides the marine absorption mostly due to CDOM, and, in coastal regions with rivers, is a good indicator of lower salinity water (Incze and Yentsch, 1981; Yentsch and Phinney, 1997). The low-salinity water mass is distinguishable from shelf waters in MERIS QAA marine absorption product, as seen in both colored imagery and grayscale (Fig. 3D & E). The nearshore zone has sufficiently high CDOM to lead to negative reflectances in the blue bands used in the algorithm, leading to algorithm failure (gray along the coast in Fig. 3A-C, and darker gray in D &E). This "saturation" corresponded to absorption greater than about 0.56 m^{-1}. The blooms on July 6 occurred mostly on water mass edge identified by absorption of 0.15 m^{-1}, and mostly near and offshore of the 100-m isobath southwest of Boothbay Harbor. By July 9, the bloom patches moved closer to the coast (Fig. 1). The CoM had moved about 50 km onshore. The 0.15 m^{-1} CDOM contour also moved onshore, although the patches had shifted to fall along the 0.56 m^{-1} absorption boundary (lower panel, Fig. 3). During downwelling, we would expect the surface water to move more rapidly onshore than the deeper water mass. By July 12, the freshwater, as shown by the absorption and water color (Fig. 5), moved downstream while further expanding offshore (Figs. 3& 4). The offshore expansion was also apparent in both MODIS Terra and Aqua products (not shown). The coherent cross-shelf movement of the dense bloom patches along the edges of low-salinity water masses suggests the coupling between physical and biological processes during the event.

SST. Throughout the event, there was no consistent SST pattern in MODIS (Fig. S3), and SST fronts did not correspond to either CDOM fronts or chlorophyll patches. The lack of thermal gradients in MODIS SST is not surprising, as thermal fronts in this region are not as evident in summer months compared to other seasons (Ullman and Cornillon, 1999). Density fronts during spring and summer are more associated with salinity differences rather than temperature (Yentsch and Phinney, 1997). Temperature fronts, if they occur, should track salinity fronts in the coastal Gulf of Maine, as salinity is more likely to define water masses and density; a salinity difference of only 1 produces the same density change as a temperature difference of 4 °C. The QAA product shows the likely salinity gradients, with the low-salinity coastal waters clearly distinguished from the shelf waters (Fig. 3).

4.2. Model results

In the first three experiments, the model was initiated with the July 06 concentration field (in relative units) derived from the MERIS data (Fig. 1). Because we initiated the bloom from the satellite imagery, to

Table 1
Numerical simulation experiments carried out in this study. The model switches (swimming and wind forcing), time period of each simulation, and model initial condition are shown.

Experiments	Swimming	Wind Forcing	Simulation Period	Initial Condition for Cell Concentration
1. Swimming+Wind	ON	ON	July 6–12	MERIS
2. No Swimming+Wind	OFF	ON	July 6–12	MERIS
3. Swimming+No Wind	ON	OFF	July 6–12	MERIS
4. Sensitivity Run	ON	ON	June 25-July 12	Uniform everywhere

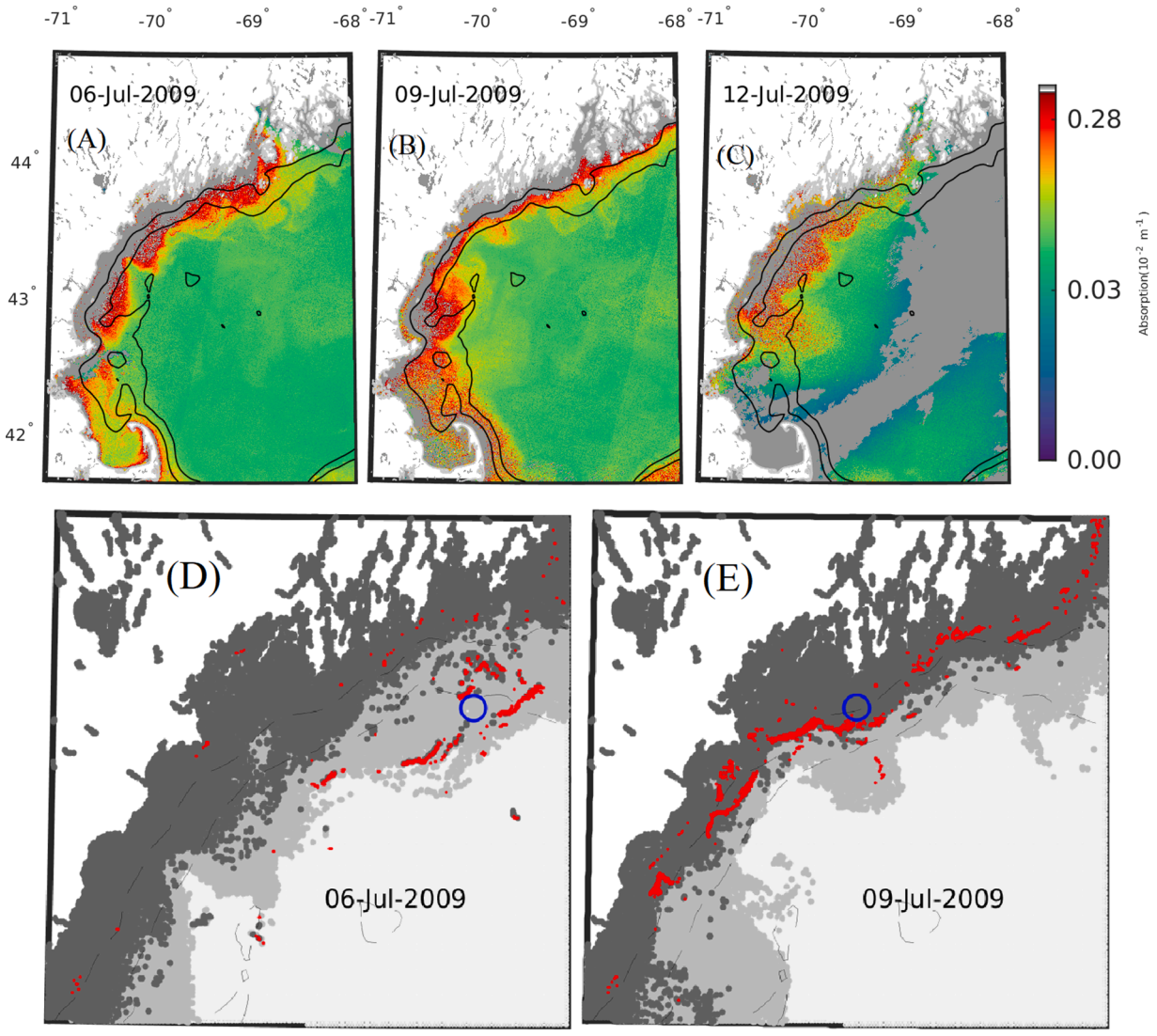

Fig. 3. (Upper) MERIS spectral marine absorption due to CDOM and detrital material (colored dissolved and particulate organic matter), QAA algorithm on (A) 6 July, (B) 9 July, and (C)12 July 2009. Land is masked as white, and cloud and invalid data are masked as gray. (Lower) zoom-in view of the spectral marine absorption for (D) July 6 and July 9, 2009 but color coded in greyscale, with waters closer to the coast (high absorption) in darker gray. Overlaid red dots are locations for simultaneous MERIS patches with chlorophyll concentration of greater than > 10 μg L^{-1}. Blue circles on July 6 and July 9 represent the center of mass in MERIS-derived chlorophyll, same as in bottom row of Fig. 4. The center of mass is derived by calculating the weighted position of the relative concentration, i.e., $CoM=\Sigma(CX)/\Sigma(X)$, where C is the tracer concentration, and X is the geographic location of each individual cell. (For interpretation of the references to colour in this figure legend, the reader is referred to the web version of this article.)

ensure the cells are conserved in mass, it is necessary to use depth-integrated cell concentration in the model to compare with satellite counterparts. The evolution of depth-integrated model solutions is shown in Fig. 5. To better illustrate the spatial movement of the cells, the centers of mass (CoM) of the concentration field in both model results and MERIS observations were derived to represent the movement of the patchy distribution of cells during the event.

The red water was observed/initialized offshore. The first model simulation considered upward swimming and was driven by realistic surface forcing (Swimming+Wind, topmost row in Fig. 5). This run reasonably reproduced the onshore and downstream motion of concentration field as observed, except for a "blob" of high concentration offshore Southeast of Casco Bay. Highest model-simulated cell concentrations were generally confined to the coastal zone with depth shallower than 50-m, although the CoM was only slightly downstream (within Casco Bay) compared to observed (near the northern end of Casco Bay). Nevertheless, when compared to the spatial pattern on July 6, the CoMs on July 9 in both Swimming+Wind experiment and MERIS travelled downstream from the 100-m isobath south of Penobscot Bay to coastal zones shallower or near 50-m isobath. The second model run (No Swimming+Wind, second row from the top in Fig. 5) showed a similar spatial pattern in the western Gulf of Maine as in the first run. Cells were aggregated at the mouth of Casco Bay while they were more evenly distributed in coastal waters further downstream (water depth <50 m). The CoM of cells is almost identical as in the first run, suggesting that upward swimming has little impact in modulating the lateral transport of the cells. The third model sensitivity run without wind (Swimming+No Wind, third row from the top in Fig. 5) showed higher concentrations of cells further offshore compared to the first and second runs, hence much fewer cells onshore. As a result, CoM in this run was located offshore on the 100-m isobath. These results suggest that wind forcing played a major role determining cell transport.

After July 9, wind shifted from downwelling-favorable to upwelling-favorable. The realistic model run (Exp. 1, Swimming+Wind) showed continued southward and offshore movement of cells. While during July 6–9 the high concentrations of cells were confined near coast, by July 12

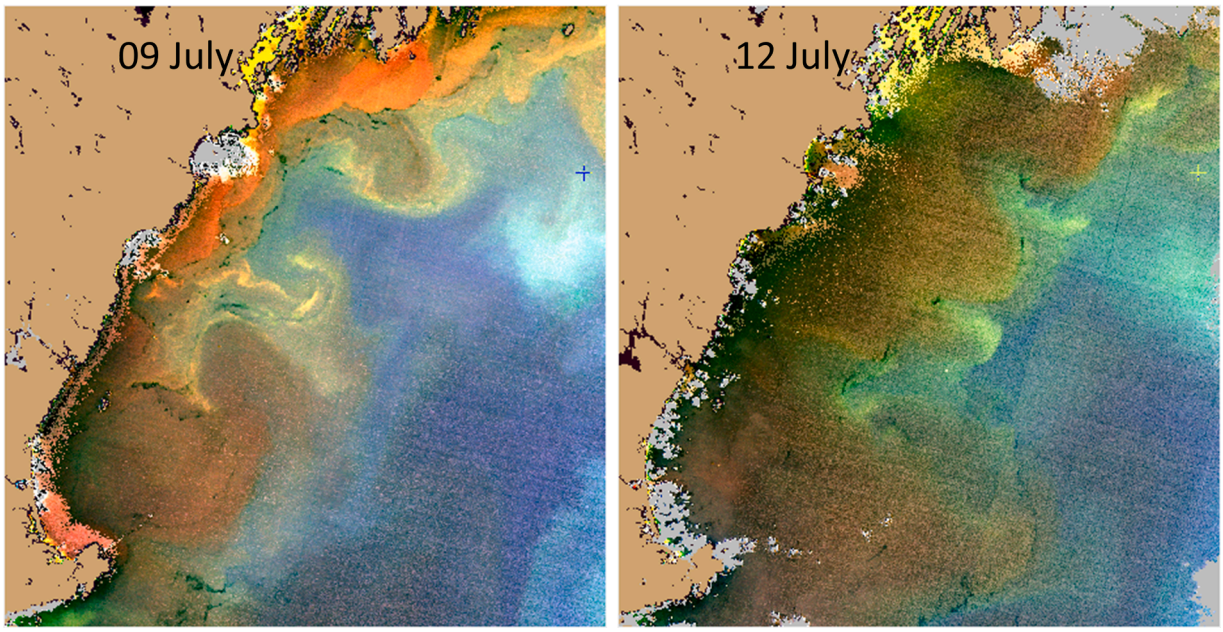

Fig. 4. Simulated RGB "true color" image produced from 300-m MERIS atmospherically corrected remote sensing reflectance. Land is masked in tan, and clouds (near shore) are masked in gray. Colored dissolved pigments from the river colors the lower salinity coastal water reddish-brown (Yentsch and Phinney, 1997). The pair shows the expansion of the discolored water offshore from 09 July to 12 July 2009, consistent with the upwelling event described in the text. (For interpretation of the references to colour in this figure legend, the reader is referred to the web version of this article.)

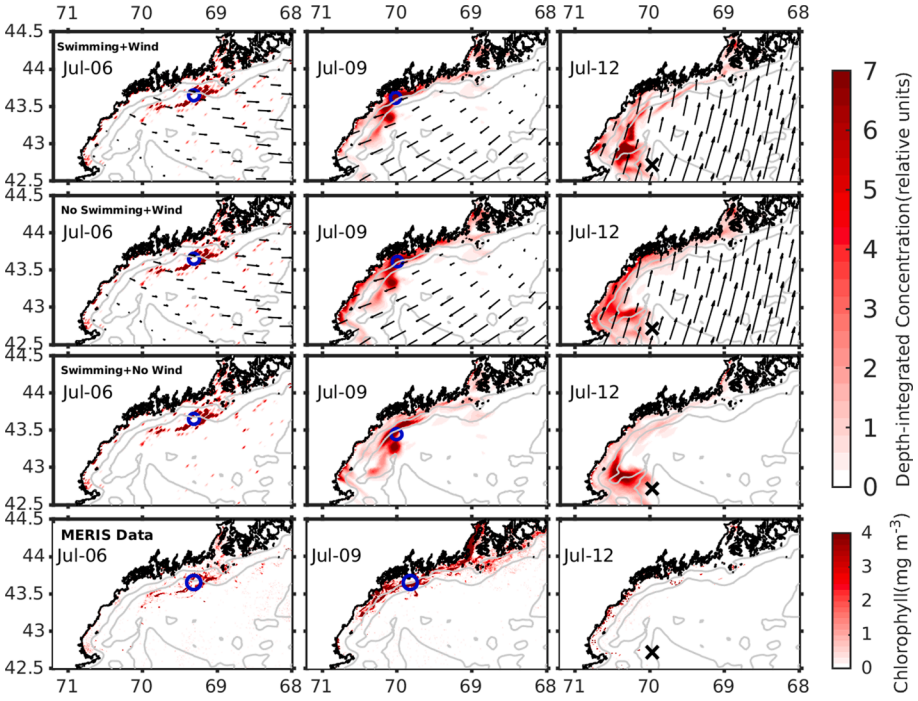

Fig. 5. Evolution of model-simulated tracer concentrations (depth-integrated) by experiments using: realistic forcing with upward swimming (Swimming+Wind, top row), realistic forcing but without swimming (No Swimming+Wind, second row from the top), and with upward swimming but without wind forcing (Swimming+No Wind, third row from the top), respectively during July 06- July 12, 2009. The blue open circles on July 6 and 9 represent the center of mass for the biological tracers, as a means to measure the tracer movement. The center of mass is derived by calculating the weighted position of the relative concentration, i.e., $CoM=\Sigma(CX)/\Sigma(X)$, where C is the tracer concentration, and X is the geographic location of each individual cell. Bottommost row stands for the MERIS-derived chlorophyll concentrations for the same period. Black crosses on rightmost column show the location of sediment trap in Wilkinson Basin during July 9–19. In each panel, gray contours highlight 50, 100, and 200-m isobaths. (For interpretation of the references to colour in this figure legend, the reader is referred to the web version of this article.)

MERIS observations showed negligible cells in coastal waters. In the meantime, while wind directions reversed, the coastal "brown" water, which is colored from the land-based CDOM (and some algae), expanded largely offshore from July 9 to July 12 (Fig. 4). Although saturated (or failing because of extremely low reflectance) near the coast, the QAA product by both MERIS (Fig. 3) and MODIS (not shown) showed substantial offshore expansion of high CDOM water during this period of upwelling-favorable wind. At this time, all three simulations showed more cells in the western Gulf than satellite imagery would suggest, especially at the offshore northeast of Cape Ann (Fig. 5).

The model has no source or sink terms, so cells are conserved. July 12 shows a substantial inconsistency between model and observations with negligible cells indicated in the satellite imagery (Fig. 1& Fig. 5). While the model-data-difference was more apparent when swimming behavior was included, even the passive model (Exp. 2, No Swimming+Wind) showed more cells than indicated from satellite. This difference is an indicator of loss of cells from the surface water, and likely loss from the water column. In the meantime, field data (Fig. 1 of McGillicuddy et al., 2014) showed low cell concentrations in the western Gulf north of Cape Ann (black cross in Figs. 1& 5), and cyst deposition was observed near

Wilkinson Basin (McGillicuddy et al., 2014). The possible processes responsible for the cell loss will be discussed in the next section.

As discussed above, coastal downwelling during July 6–9 facilitated onshore movement and aggregation of the cells, thereby allowing the formation of highly concentrated patches near coastal zones. Cross-shore transport of the biological patch was consistent with the movement of salinity-dominated coastal water mass. Wind from late June to July 9, 2009 produced an unusually persistent coastal downwelling event compared to the same time periods in other years from 2004 to 2011 (Fig. 2). To quantify the contribution of upward swimming to cell aggregations, we initiated the model from June 25, 2009 (to include the unusual downwelling event in June) with a uniform cell concentration everywhere, and compared the resulting depth-integrated cell concentration with and without upward swimming (Exp.4 in Table 1). The swimming case aggregates more cells than the case without swimming (Fig. 6). In the swimming case, the concentration reached a maximum at mid-day of July 3 (Fig. 7A). The persistent coastal downwelling (Fig. 7B) from late June up until July 3 combined with the upward swimming to promote cell accumulation. A sporadic reversal to upwelling-favorable wind lowered the concentration until July 6, before downwelling re-accumulated the cells near the coast. The weak upwelling-favorable wind during July 9–12 slightly reduced the concentration to ~20-fold that of the initial condition. The maximum depth-integrated cell concentration during aggregation for the swimming case was up to 40 times the magnitude for the no-swimming case (Fig. 7A), qualitatively consistent with Franks et al. (1997), who found a clear link between frontal aggregation and upward swimming velocity.

5. Discussion

Importance of upward swimming to cell accumulation of A. catenella. The swimming behavior of dinoflagellates produces systematic movement through the water column (Tyler and Seliger, 1981; Kamykowski, 1981; Anderson and Stolzenbach, 1985; Franks, 1992; Smayda, 2002). Positive phototaxis leads to accumulations in surface waters and particularly to accumulations at oceanic fronts (e.g., Incze and Yentsch, 1981; Seliger et al., 1979; Tyler et al., 1985; Tyler and Stumpf, 1989; Franks, 1992; Pitcher et al., 1998; Litaker et al., 2002; Stumpf et al., 2008). Modeling studies have explained this accumulation through the combination of swimming activity and physical circulation transport (Franks, 1992; 1997; Hetland, 2007; Janowitz and Kamykowski, 2006; Stumpf et al., 2008). Including swimming within fully three-dimensional population models is essential to correctly model the distributions of these blooms.

Stumpf et al. (2008) studied the aggregation of *K. brevis* cells near the inner shelf front along Southwest Florida identified from satellite data. On January 2 of 2005, cells were evenly distributed along the coast. Cells were subsequently advected to the south, and accumulated along the front by January 6. From January 6 to 8, bloom magnitude increased up to 10-fold within a period of 1–2 days, which could not be explained by local cell growth (typically less than 1 doubling per day). A convergence by physical circulation along with nutrient-seeking active swimming (Janowitz and Kamykowsi, 2006) may work in concert to favor *K. brevis* accumulation. Similarly, as physical and biological processes are coupled, here we can estimate the bloom aggregation combining directional swimming behavior and physical circulation using numerical model simulations.

Under normal bloom conditions *A. catenella* reaches concentrations of several hundred to a thousand cells L^{-1} (Smayda, 1997). The red water event in 2009, however, produced a bloom with concentrations from hundreds of thousands to 1 million cells L^{-1} (McGillicuddy et al., 2014). This is a 1000-fold increase in cell concentrations. The 40-fold increase in initial cell concentrations as discussed above can be accounted for by the frontal aggregation due to horizontal convergence

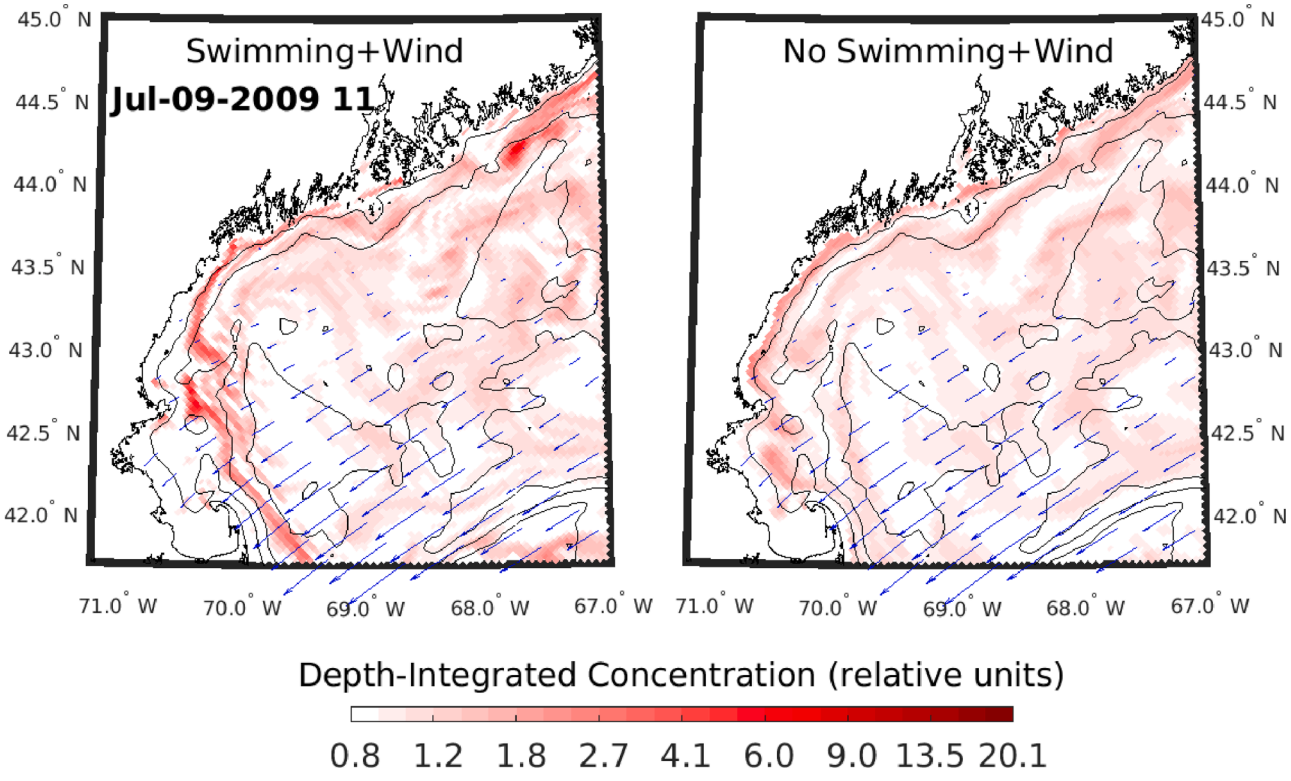

Fig. 6. Simulated cell concentrations for July 09, 2009 at 11am local time for model experiment 4 in Table 1. The model was initiated on June 25, 2009 with uniform depth-integrated concentrations over the model domain. Note that the color scale is nonlinear. Gray contours highlight 50, 100, and 200-m isobaths, and blue vectors show the simultaneous wind stress at the surface. (For interpretation of the references to colour in this figure legend, the reader is referred to the web version of this article.)

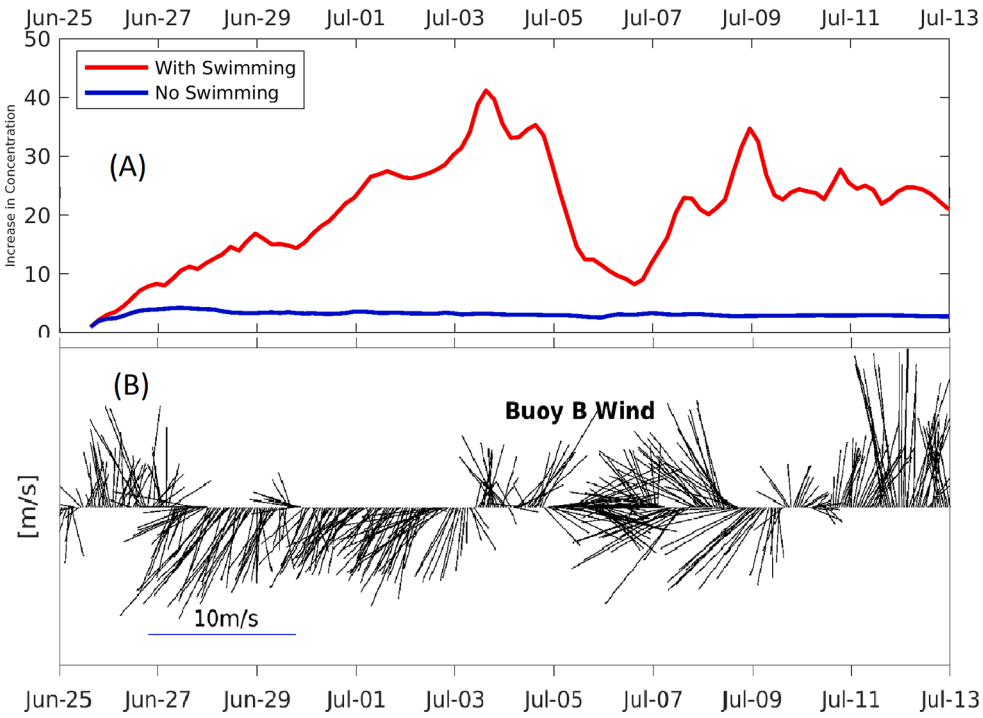

Fig. 7. (A) Time series of the model (experiment 4 in Table 1) simulated domain-wide maximum of depth-integrated concentrations normalized by the model initial concentration for swimming (red) and no-swimming (blue) cases during June 25- July 13, 2009. The model was initialized on June 25, 2009 with uniform depth-integrated concentrations over the model domain. (B) Temporal evolution of wind speed at NERACOOS buoy B during the same period. A scaling factor of 10 m/s for wind speed is also shown. (For interpretation of the references to colour in this figure legend, the reader is referred to the web version of this article.)

in the presence of upward swimming; yet another factor of 25 (25×40= 1000-fold) is needed to achieve the concentrations that discolor the water.

One possible mechanism that accounts for the 25-fold discrepancy is vertical aggregation from subsurface to the surface layer due to vertical swimming. To examine this process, we re-examined the sensitivity experiment with initiation on June 25 (Exp. 4 in Table 1). The experiment compared swimming and no-swimming cases to produce the vertical evolution of the cell concentrations, sampled at NERACOOS buoy B in the western Gulf of Maine (Fig. S3). Without directional upward swimming (mid panel in Fig. S3), a high density of cells at the surface layer were dispersed over the water column as deep as 20-m during strong mixing events. In contrast, when swimming was considered, the cell concentrations were restrained to the top 1–2 m layer, greatly reducing the vertical dispersion of the cells. Surface layer concentration in the swimming case was up to 90-fold compared to the non-swimming case. Note that the results presented herein were not strictly one dimensional, as horizontal accumulation of cells (as stated in discussion section, e.g., Fig. 5), may also contribute to the surface cell accumulation. Nevertheless, it is clear that upward swimming facilitates vertical convergence of the cells, preventing the cells from being mixed with low-concentration waters at depth. The vertical convergence of cells near the surface could account for the additional factor of 25 (e.g., concentration over 25 m aggregated to a 1-m layer) in the observed cell concentration. This result indicated that discolored surface water due to the accumulation of cells through vertical convergence combined with horizontal convergence was possible.

Our results are consistent with various previous studies, which found that upward swimming is effective in aggregating cells in the vertical layer. Using in situ observations, Pingree et al. (1975) found that under stratified water conditions, surface layer biomass containing red tide cells can be up to 40 times higher than at depth, a process associated with swimming behavior. Tyler et al. (1983) found concentrations >100-fold greater at surface than only a few meters below the surface. Glider observations of the dinoflagellate *K. brevis* show that the bloom concentrations can increase by ~20 times in a day, a process due to active vertical swimming (Qi et al., 2017). Similarly, Schofield et al. (2016) used Lagrangian drifters to observe changes in optical characteristics resulting from vertical swimming. We should note that while aggregation of cells does not require active local growth (Carreto et al., 1986; Franks, 1992; Smayda, 2002), nutrients supplied by physical circulation near the frontal zone may also fuel growth of the bloom in associated biological patches (e.g., Janowitz and Kamykowski, 2006; Heil et al., 2014).

Implication for bloom dynamics. Because there is no source or sink term in the model, the discrepancies between model solutions and satellite data can be a good indicator of loss of cells from the system. The modeled cell concentrations in July 12 showed much higher cell concentration than observed in the field (McGillicuddy et al., 2014) as well as by satellite (Fig. 3). While the difference was more apparent when swimming was included, even the passive model (No Swimming+Wind) predicted more cells than were observed. The discrepancy indicated that there was loss of cells from the water column later in the event. There are at least three processes that may be responsible for such a cell loss. One possible mechanism is the removal of *A. catenella* cells due to grazing pressure by zooplankton, or the mortality of cells themselves due to other factors, e.g., viruses, or parasitism (Velo-Suárez et al., 2013). The second primary mechanism is loss by encystment following sexual reproduction. Under environmental pressure, such nutrient depletion, the cells combine to form gametes/zygotes, leading to the cysts that settle into sediment layer. The accumulation and aggregation of cells (that causes the discolored water) may favor sexual reproduction by proximity, thereby being a precursor of the encystment process. Indeed, sexual reproduction did occur during the 2009 red water events (McGillicuddy et al., 2014). Therefore, it may be possible to identify the potential of encystment by combining observations, numerical models, and satellite imagery. Finally, the third mechanism for loss, could be episodic mixing that may reduce the surface concentration of cells detectable by satellite on July 12. However, accumulations did not appear again in the satellite imagery in July, indicating this mechanism is insufficient to explain the loss of cells. In addition, with upward swimming, model results showed that cells mostly aggregate within the upper 1–2 m of the water column. Mixing alone is unlikely to be the mechanism explaining the loss, particularly when the cells did not reappear at the surface.

The biological model used here does not have a term to allow for

variability in reproduction or loss due to encystment. Pilskaln et al. (2014) measured cyst fluxes every 10 days at 95 m and 180 m at Wilkinson Basin (black cross in Fig. 1). The cyst accumulation period started July 9 and continued until August 19. At 95 m, the flux peaked during the period July 9–19; this was coincident with the timing of arrival of cells to the Wilkinson Basin (WB in Fig. 1, also in Fig. 5) and is coincident with the loss shown by satellite against the model. Given the contrast of model and observations, the delivery of the cells to the location may provide an estimate for the timing of the encystment processes.

The results presented here have some implications for *A. catenella* predictions. There are at least two important factors in determining the intensity of *A. catenella* blooms: physical accumulation because of the coupling of swimming and fluid dynamics, and mechanism accounting for removal of cells from water column—including encystment. Physical accumulation processes may help identify areas that face greater risk of high toxicity; namely that areas that favor cell accumulation may end up with more cells than would occur in areas without them, and the location of cell accumulation zones varied with the wind forcing (Figs. 3, Fig. 5, July 9). Gulf-wide, observations show that the red water in 2009 appeared to have been the southern terminus of a coast-wide event, leading to the widespread toxicity from Bay of Fundy to the western Gulf of Maine.

It is unknown what the grazing pressure was during the red water event, nor whether grazers responded fast enough to impact the accumulation. In a prior study, Turner (2010) found that in most cases grazing and growth were in balance, but when *Alexandrium* cell concentrations were $>10^4$ cells L^{-1}, cell growth exceeded grazing losses by zooplankton community. However, the role of grazing in bloom demise remains unclear. In our case, while it is not impossible that grazing contributed to termination of the bloom, the encystment event following the peak bloom on July 9 suggested that encystment can lead to a rapid loss of cells from the system. Thus, identifying the timing of the encystment would aid in forecasting the end of a bloom. Samples at the time indicated that sexual reproduction was occurring (McGillicuddy et al., 2014). Accumulation of cells favors occurrence of sexual reproduction, both through physical contact and through nutrient stress, as seen in laboratory experiments (Anderson, 1998). However, the trigger for cyst formation in natural *A. catenella* populations remains unresolved (Anderson et al., 1984; Anderson and Lindquist, 1985; Turpin et al., 1978; McGillicuddy et al., 2005). As such, predictability of the encystment process remains a research question.

6. Conclusions

A red water event of *Alexandrium catenella* took place in July 2009 in Gulf of Maine. The bloom initiated offshore, moved onshore, and diminished within a week. The position of an A. *catenella* bloom patch showed coherence with the coastal, typically low-salinity water. SST provides less information, and there were no SST features related to bloom patches. This event provided an opportunity to obtain spatial and temporal information that is not commonly available for *A. catenella*. Numerical model simulations combined with satellite imagery was used to understand the importance of surface wind forcing and vertical swimming during the event.

In the early stage of the event (i.e., onshore transport), model simulations suggested that the downwelling-favorable wind was critical in transporting cells onshore during July 6–9. Further model results showed that upward swimming can facilitate cell accumulation by ~40-fold by horizontal convergence, suggesting that swimming behavior may play an important role in forming such a red-water event. While a 40-fold increase relative to a normal bloom condition is insufficient to discolor the water, another factor of 25 may come from vertical convergence due to directional swimming toward the surface layer, as suggested by our research (and others) on dinoflagellates.

During July 9–12, the model showed more cells than either observed in the field (McGillicuddy et al., 2014) or estimated from satellite. Thus, modeling experiments provided evidence that rapid loss of cells might respond to the timing of significant encystment in the western Gulf of Maine. Our work also suggested that dense accumulations of cells (which may discolor the water) may be a precursor for encystment. One of the major challenges of forecasting the *A. catenella* is determining the cyst abundance in the sediments prior to the start of a bloom season. Currently, that process is done through expensive shipboard sampling. Continued research to promote the understanding of encystment may lead to reduced effort in the cyst sampling requirement.

Satellite imagery introduces a new capability in monitoring these blooms. Because *Alexandrium* species do not typically dominate the biomass in areas where they pose a health risk, the prevailing view has been that satellite imagery is not useful for these blooms. As a practical matter, McGillicuddy et al. (2014) noted that observing the intense bloom from ship was “serendipitous”. Satellite observations support that observation – two days later the high concentration patches were no longer visible. Satellite data available to McGillicuddy et al. (2014) lacked the resolution (1 km) to see or distinguish cell accumulations, but also was limited by the standard blue-green band ratio algorithms that do not readily distinguish chlorophyll from CDOM. The MERIS full resolution imagery, when it was available from 2002 to 2012, could provide an order of magnitude more spatial resolution than other commonly available ocean color satellites, as well as bands that allow specificity to chlorophyll detection. Since the 2016 launch of the Copernicus program’s Sentinel-3 satellite, the Ocean Land Colour Imager (OLCI) has provided an equivalent data stream, with up to daily coverage when Sentinel-3b becomes available in 2019 (vs. 3 days for MERIS). However, the “serendipity” that occurred for this event suggests that other years should be re-examined for similar aggregations. Similar events may be examined for future years as well. The combination of satellite data and modeling expands the options for examining intensification and decline of these blooms.

Declaration of Competing Interest

The authors declare that they have no known competing financial interests or personal relationships that could have appeared to influence the work reported in this paper.

Acknowledgements

We are grateful to NASA GFSC and the European Space Agency for making the Level 1 MERIS and MODIS data available. YL’s time at WHOI was supported by the Postdoctoral Scholarship Program at Woods Hole Oceanographic Institution, with funding provided by the Dr. George D. Grice Postdoctoral Scholarship. YL’s NOAA time is supported by NOAA NCCOS HAB Forecast project. YL and RPS thank Andrew Meredith for help processing satellite imagery. YL are also grateful to Timothy Wynne, Danielle Dupuy, and Michelle Tomlinson for the useful inputs during NOAA internal reviews. DJM gratefully acknowledges support of the Woods Hole Center for Oceans and Human Health, funded jointly by the National Science Foundation (OCE-1314642 and OCE-1840381) the National Institute of Environmental Health Sciences (P01ES021923–01 and P01 ES028938–01). RH acknowledges support made possible by NOAA grant NA15NOS4780196 and NA16NOS0120028. We are indebted to Editor Raphael Kudela and three anonymous reviewers for providing insightful comments that greatly improved the quality of the manuscript.

Supplementary materials

Supplementary material associated with this article can be found, in the online version, at doi:10.1016/j.hal.2020.101927.

References

Anderson, D.M., Kulis, D.M., Binder, B.J., 1984. Sexuality and cyst formation in the dinoflagellate Gonyaulax tamarensis: cyst yield in batch cultures. J. Psychol. 20, 418–425.

Anderson, D.M., Lindquist, N.L., 1985. Time-course measurements of phosphorous depletion and cyst formation in the dinoflagellate Gonyaulax tamarensis Lebour. J. Exp. Mar. Biol. Ecol. 86 (1), 1–13.

Anderson, D.M., Stolzenbach, K.D., 1985. Selective retention of two dinoflagellates in a well-mixed estuarine embayment: the importance of diel vertical migration and surface avoidance. Mar. Ecol. Prog. Ser. 25, 39–50.

Anderson, D.M., Kulis, D.M., Sullivan, J.J., Hall, S., Lee, C., 1990. Dynamics and physiology of saxitoxin production by the dinoflagellates Alexandrium spp. Mar. Biol. 104 (3), 511–524.

Anderson, D.M., 1998. Physiology and bloom dynamics of toxic Alexandrium species, with emphasis on life cycle transitions. Nato Asi Series G Ecol. Sci. 41, 29–48.

Anderson, Donald M., et al., 2005a. Initial observations of the 2005 Alexandrium fundyense bloom in southern New England: general patterns and mechanisms. Deep Sea Res. Part II 52 (19–21), 2856–2876.

... & Anderson, D.M., Stock, C.A., Keafer, B.A., Nelson, A.B., Thompson, B., McGillicuddy Jr., D.J., Martin, J., 2005b. Alexandrium fundyense cyst dynamics in the Gulf of Maine. Deep Sea Res. Part II 52 (19–21), 2522–2542.

Balch, W.M., Drapeau, D.T., Bowler, B.C., Booth, E.S., Goes, J.I., Ashe, A., Frye, J.M., 2004. A multi-year record of hydrographic and bio-optical properties in the Gulf of Maine: I. Spatial and temporal variability. Progr. Oceanogr. 63 (1–2), 57–98.

Balch, W., Huntington, T., Aiken, G., Drapeau, D., Bowler, B., Lubelczyk, L., Butler, K., 2016. Toward a quantitative and empirical dissolved organic carbon budget for the Gulf of Maine, a semienclosed shelf sea, Global Biogeochem. Cycles 30, 268–292. https://doi.org/10.1002/2015GB005332.

Belkin, I.M., O'Reilly, J.E., 2009. An algorithm for oceanic front detection in chlorophyll and SST satellite imagery. J. Marine Syst. 78 (3), 319–326.

Carreto, José I., et al., 1986. 1986: toxic red-tide in the Argentine Sea. Phytoplankton distribution and survival of the toxic dinoflagellate Gonyaulax excavata in a frontal area. J. Plankton Res. 8 (1), 15–28.

Franks, P.J.S., 1992. Sink or swim: accumulation of biomass at fronts. Mar. Ecol. Prog. Ser. 82, 1–12.

15 Franks, P.J.S., and Anderson, D.M. m1992. Alongshore transport of a toxic phytoplankton bloom in a buoyancy current: alexandrium tamarense in the Gulf of Maine. Mar. Biol., 112(1), 153–164.

Franks, P.J., 1997. Spatial patterns in dense algal blooms. Limnol. Oceanogr. 42 (5), 1297–1305.

Gilerson, A.A., Dall'Olmo, G., Moses, W., Rundquist, D.C., Barrow, T., Fisher, T.R., Gurlin, D., Holz, J., 2008. A simple semi-analytical model for remote estimation of chlorophyll-a in turbid waters: validation. Remote Sens Environ 112, 3582–3593.

Gower, J., King, S., Borstad, G., Brown, L., 2005. Detection of intense plankton blooms using the 709 nm band of the MERIS imaging spectrometer. Int. J. Remote Sens. 26 (9), 2005–2012.

Hetland, R.D., Signell, R.P., 2005. Modeling coastal current transport in the Gulf of Maine. Deep Sea Res. Part II 52 (19–21), 2430–2449.

Hetland, R.D., Campbell, L., 2007. Convergent blooms of *Karenia brevis* along the Texas coast. Geophys. Res. Lett. 34, L19604, 10.1029/2007GL030474.

He, R., McGillicuddy, D.J., 2008. Gulf of Maine Harmful algal bloom in summer 2005-Part 1: in situ observations of coastal hydrography and circulation. J. Geophys. Res. 113 (C7).

He, R., McGillicuddy, D., Keafer, B., Anderson, D., 2008. Gulf of Maine Harmful Algal Bloom in Summer 2005: part 2. Coupled biophysical modeling. J. Geophys. Res. 113, C07040, 10.1029/2007JC004602.

Hyun, K.H., He, R., 2010. Coastal upwelling in the South Atlantic Bight: a revisit of the 2003 cold event using long term observations and model hindcast solutions. J. Marine Syst. 83, 1–13.

Incze, L.S., Yentsch, C.M., 1981. Stable density fronts and dinoflagellate patches in a tidal estuary. Estuar Coast Shelf Sci 13 (5), 547–556.

Janowitz, G.S., Kamykowski, D., 2006. Modeled *Karenia brevis* accumulation in the vicinity of a ccoastal nutrient front. Mar. Ecol. Prog. Ser. 314, 49–59.

Jin, D., Hoagland, P., 2008. The value of harmful algal bloom predictions to the nearshore commercial shellfish fishery in the Gulf of Maine. Harmful Algae 7 (6), 772–781.

Kamykowski, D., Reed, R.E., Kirkpatrick, G.J., 1992. Comparison of the sinking velocity, swimming velocity, rotation and path characteristics among six marine dinoflagellate species. Mar. Biol. 113 (2), 319–328.

Keafer, B.A., Churchill, J.H., McGillicuddy, D.J., Anderson, D.M., 2005. Bloom development and transport of toxic Alexandrium fundyense populations within a nearshore coastal plume in the Gulf of Maine. Deep-Sea Research II 52, 2674–2697.

Kleindinst, J.L., Anderson, D.M., McGillicuddy Jr, D.J., Stumpf, R.P., Fisher, K.M., Couture, D.A., Hickey, J.M., Nash, C., 2014. Categorizing the severity of paralytic shellfish poisoning outbreaks in the Gulf of Maine for forecasting and management. Deep Sea Res. Part II 103, 277–287.

Lee, Z., Carder, K.L., &Arnone, R.A., 2002. Deriving inherent optical properties from water color: a multiband quasi-analytical algorithm for optically deep waters. Appl. Opt. 41 (27), 5755, 10.1364/ao.41.005755.

Lee, Z., Lubac, B., Werdell, J., Arnone, R., 2009. An update of the quasi-analytical algorithm (QAA_v5). Int. Ocean Color Group Softw. Rep. 1–9.

Le Fevre, J., 1987. Aspects of the Biology of Frontal systems. In Advances in Marine Biology, 23. Academic Press, Vol, pp. 163–299.

Li, Y., He, R., McGillicuddy, D., Anderson, D., Keafer, B.A., 2009. Investigation of 2006 *Alexandrium catenella* bloom in the Gulf of Maine: in-situ observations and numerical modeling. Cont. Shelf. Res. 29, 2069–2082.

Litaker, R.W., Tester, P.A., Duke, C.S., Kenney, B.E., Pinckney, J.L., Ramus, J., 2002. dinoflagellate swimming, Seasonal niche strategy of the bloom-forming dinoflagellate *Heterocapsa triquetra*. Mar. Ecol. Prog. Ser. 232, 45–62.

Liu, Y., Heer, J., 2018. Somewhere over the rainbow: an empirical assessment of quantitative colormaps. In Proceedings of the 2018 CHI Conference on Human Factors in Computing Systems 1–12.

Love, R.C., Loder III, T.C., Keafer, B.A., 2005. Nutrient conditions during Alexandrium fundyense blooms in the western Gulf of Maine, USA. Deep Sea Res. Part II: Topical Studies in Oceanography 52 (19–21), 2450–2466.

Lou, X., Hu, C., 2014. Diurnal changes of a harmful algal bloom in the East China Sea: observations from GOCI. Remote Sens. Environ. 140, 562–572.

Luerssen, R.M., Thomas, A.C., Hurst, J., 2005. Relationships between satellite-measured thermal features and Alexandrium-imposed toxicity in the Gulf of Maine. Deep Sea Res. Part II 52 (19–21), 2656–2673.

Luettich, R.A., Westerink .J., J., Scheffner, N.W., 1992. ADCIRC: an advanced three-dimensional circulation model for shelves, coasts and estuaries. U.S. Army Eng. Waterways Exp. Station.

Marchesiello, P., McWilliams, J.C., Shchepetkin, A.F., 2001. Open boundary conditions for long-term integration of regional oceanic models. Ocean Modell. 3, 1–20.

McGillicuddy, D.J., Signell, R.P., Stock, C.A., Keafer, B.A., Keller, M.D., Hetland, R.D., Anderson, D.M., 2003. A mechanism for offshore initiation of harmful algal blooms in the coastal Gulf of Maine. J. Plankton Res. 25, 1131–1138.

McGillicuddy, D.J., Anderson, D.M., Lynch, D.R., Townsend, D.W., 2005. Mechanisms regulating the large-scale seasonal fluctuations in *Alexandrium catenella* populations in the Gulf of Maine: results from a physical-biological model. Deep-Sea Res. II 52, 2698–2714.

McGillicuddy, D.J., Brosnahan, M.L., Couture, D.A., He, R., Keafer, B.A., Manning, J.P., Martin, J.L., Pilskaln, C.H., Townsend, D.W., Anderson, D.M., 2014. A red tide of *Alexandrium catenella* in the Gulf of Maine. Deep-Sea Res. II 103, 174–184.

Moses, W.J., Gitelson, A.A., Perk, R.L., Gurlin, D., Rundquist, D.C., Leavitt, B.C., Barrow, T.M., Brakhage, P., 2012. Estimation of chlorophyll-a concentration in turbid productive waters using airborne hyperspectral data. Water Res. 46 (4), 993–1004.

Pilskaln, C.H., Anderson, D.M., McGillicuddy, D.J., Keafer, B.A., Hayashi, K., Norton, K., 2014. Spatial and temporal variability of Alexandrium cyst fluxes in the Gulf of Maine: relationship to seasonal particle export and resuspension. Deep-Sea Res. II 103, 40–54.

Pingree, R.D., Pugh, P.R., Holligan, P.I., Forster, G.R., 1975. Summer phytoplankton blooms and red tides along tidal fronts in the approaches to the English Channel. Nature 258 (5537), 672.

Pitcher, G.C., Boyd, A.J., Horstman, D.A., Mitchell-Innes, B.A., 1998. Subsurface dinoflagellate populations, frontal bloomsand the formation of red tide in the Southern Benguela upwelling system. Mar. Ecol. Prog. Ser. 172, 253–264.

Qi, L., Hu, C., Barnes, B.B., Lee, Z., 2017. VIIRS captures phytoplankton vertical migration in the NE Gulf of Mexico. Harmful Algae 66, 40–46.

Salisbury, J., Vandemark, D., Campbell, J., Hunt, C., Wisser, D., Reul, N., Chapron, B., 2011. Spatial and temporal coherence between Amazon River discharge, salinity, and light absorption by colored organic carbon in western tropical Atlantic surface waters. J. Geophys. Res. 116 (C7).

Schofield, Oscar, et al., 2006. Vertical migration of the toxic dinoflagellate Karenia brevis and the impact on ocean optical properties. J. Geophys. Res. 111.C6.

Seliger, H.H., Tyler, M.A., McKinley, K.R., 1979. Phytoplankton distributions and red tides resulting from frontal circulation patterns. Toxic Dinoflagellate Blooms 239–248.

Shcheptkin, A.F., McWilliams, J.C., 2005. A split-explicit, free-surface, topographic following-coordinate oceanic model. Ocean Modell. 9, 347–404.

Smayda, T.J., 1997. Harmful algal blooms: their ecophysiology and general relevance to phytoplankton blooms in the sea. Limnol. Oceanogr. 42 (5), 1137–1153.

Smayda, T.J., 2002. Turbulence, watermass stratification and harmful algal blooms: an alternative view and frontal zones as "pelagic seed banks". Harmful Algae 1 (1), 95–112.

Stock, C.A., McGillicuddy, D.J., Solow, A.R., Anderson, D.A., 2005. Evaluating hypothesis for the initiation and development of *Alexandrium catenella* blooms in the western Gulf of Maine using a coupled physical-biological model. Deep Sea Res. II 52, 2715–2744.

Stumpf, R.P., Pennock, J.R., 1989. Calibration of a general optical equation for remote sensing of suspended sediments in a moderately turbid estuary. J. Geophys. Res. 94, 14,363-14,371.

Stumpf, R.P., Tyler, M.A., 1988. Satellite detection of bloom and pigment distribution in estuaries. Remote Sens. Environ. 24, 385–404.

Stumpf, R.P., Goldschmidt, P.M., 1992. Remote sensing of suspended sediment discharge into the western Gulf of Maine during the April 1987 100-year flood. J. Coastal Res. 218–225.

Stumpf, R.P., Litaker, R.W., Lanerolle, L., Tester, P.A., 2008. Hydrodynamic accumulation of Karenia off the west coast of Florida. Cont. Shelf Res. 28, 189–213.

Velo-Suárez, L., Brosnahan, M.L., Anderson, D.M., McGillicuddy, D.J., 2013. A quantitative assessment of the role of the parasite Amoebophrya in the termination of *Alexandrium fundyense* blooms within a small coastal embayment. PLoS ONE 8 (12), 1-10, e81150.

Turner, J.T., 2010. Zooplankton community grazing impact on a bloom of Alexandrium fundyense in the Gulf of Maine. Harmful Algae 9 (6), 578–589.

Turpin, D.H., Dobel, P.E.R., Taylor, F.J.R., 1978. Sexuality and cyst formation in Pacific strains of the toxic dinoflagellate Gonyaulax tamarensis. J. Psychol. 14, 235–238.

Tyler, M.A., Seliger, H.H., 1981. Selection for a red tide organism: physiological responses to the physical environment. Limnol. Oceanogr. 26, 310–324.
Tyler, M.A., Stumpf, R.P., 1989. Feasibility of using satellites for detection of kinietcs of small phytoplankton blooms in estuaries; tidal and migrational effects. Remote Sens. Environ. 27, 233–250.
Ullman, D.S., Cornillon, P.C., 1999. Satellite-derived sea surface temperature fronts on the continental shelf off the northeast US coast. J. Geophys. Res. 104 (C10), 23459–23478.
Yentsch, C.S., Phinney, D.A., 1997. February. Yellow substances in the coastal waters of the Gulf of Maine: implications for ocean color algorithms. In Ocean Optics XIII (Vol. 2963, 120-132). Int. Soc. Opt. Photon.